Robust superhydrophobic epoxy composite coating prepared by dual interfacial enhancement

Xiguang Zhang[a,c], Zhanjian Liu[b], Yuan Li[a,c], Chijia Wang[b], Yanji Zhu[b], Huaiyuan Wang[a,b,c,*], Jingtao Wang[a]

[a] School of Chemical Engineering and Technology and State Key Laboratory for Chemical Engineering, Tianjin University, Tianjin 300350, PR China
[b] College of Chemistry and Chemical Engineering, Northeast Petroleum University, Daqing 163318, PR China
[c] Collaborative Innovation Center of Chemical Science and Engineering (Tianjin), Tianjin University, Tianjin 300072, PR China

HIGHLIGHTS

- The durable superhydrophobic coating was prepared by dual interfacial enhancement.
- The prepared superhydrophobic coating can withstand 10^5 abrasion cycles.
- The formed nano-miro-nano structure can prolong the hydrophobic lifespan in water.
- The coating exhibited highly self-cleaning and anti-fouling properties in slurry.

GRAPHICAL ABSTRACT

A durable superhydrophobic EP-PTFE/GP-SiO$_2$-POTS coating with excellent wear resistance was prepared by dual interfacial enhancement. High pressure of melt extrusion and the "glue" action of polydopamine was used to enhance interface bonding force. In addition, the formed nano-micro-nano structure on the surface established two defense lines to prolong the hydrophobic lifespan underwater.
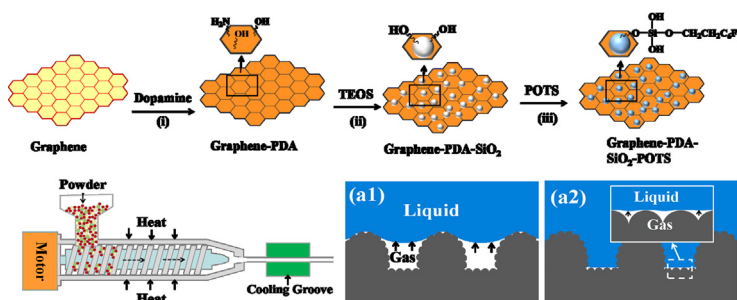
ARTICLE INFO

ABSTRACT

Superhydrophobic surfaces with special wettability have a promising potential for self-cleaning, anti-fouling, and anti-corrosion applications. However, the practical applications of superhydrophobic coatings are currently limited by their poor mechanical strength and hydrophobic durability. Here, we report a superhydrophobic epoxy (EP) composite coating with improved durability, achieved by a dual interfacial enhancement. First, melt extrusion technology was used to enhance the bonding force between EP and polytetrafluorethylene (PTFE). Then, combining dopamine self-polymerization and sol-gel approaches, the interfacial strength between graphene-polydopamine (GP) and SiO$_2$ was enhanced by in-situ growth of SiO$_2$ on the GP surface. After modification with 1H,1H,2H,2H-perfluorooctyltriethoxysilane (POTS), the superhydrophobic EP-PTFE/GP-SiO$_2$-POTS coating (WCA = 156.3 ± 1.5°, WSA = 3.5 ± 0.5°) was successfully prepared on a steel surface by electrostatic spraying. With the enhanced interfacial strength, the prepared composite coating demonstrated excellent mechanical performance, and could withstand 10^5 abrasion cycles with only 54.4 mg weight loss. Moreover, due to the induction effect of graphene, a special multilayered nano-micro-nano structure was formed by the evenly distributed nano-SiO$_2$ particles on the coating surface, which is beneficial to extend its super-hydrophobic duration. The prepared coating can maintain its superhydrophobicity even after being scratched or

* Corresponding author at: School of Chemical Engineering and Technology and State Key Laboratory for Chemical Engineering, Tianjin University, Tianjin 300350, PR China.
  E-mail address: huaiyuanwang@tju.edu.cn (H. Wang).

immersed in 3.5 wt% NaCl solution for 60 days. Therefore, the prepared superhydrophobic coating demonstrates great potential for application in anti-fouling, drag reduction, and other fields.

1. Introduction

Lotus leaf-inspired superhydrophobic coatings are generally characterized by a water contact angle (WCA) higher than 150° and a water sliding angle (WSA) lower than 10° [1]. The wide potential applications of the superhydrophobic surfaces, such as anti-fogging [2], anti-ice [3], and self-cleaning [4], as well as selective absorption [5] and drag reduction [6], have attracted considerable attention. In the past two decades, thousands of artificial superhydrophobic surfaces have been prepared by designing the surface microstructure or adjusting the surface free energy [7–9]. However, their hydrophobic stability and mechanical performance in practical applications are often inadequate, which limits their large-scale use [10,11]. As is well known, the durability of superhydrophobic coatings mainly depends on the surface hierarchical structure and low surface energy materials [12]. Based on the Wenzel and Cassie-Baxter models, low surface energy materials can impart hydrophobicity to a coating and the hierarchical structure can trap microscopic pockets of air to reduce the contact area between water drops and coating surface, leading to an increased WCA and a reduced WSA [13].

Currently, the main routes to enhance the durability of the superhydrophobic coatings involve designing robust hierarchical structures and regenerating the surface compositions [14]. However, the superhydrophobic durability against abrasion or corrosion damages is still poor. When the surface structure or the low surface energy materials is destroyed, the stability of the air film trapped by the hydrophobic hierarchical structure decreases, resulting in a poor hydrophobic durability under water. Accordingly, various efforts have been mad to improve the stability of the air film. Cheek et al. [15] replenished hydrogen on a conductive superhydrophobic surface by an electrolytic reaction compensation method. Under a voltage of 2.0 V and a current of 0.225 mA, the superhydrophobic durability was enhanced by 400%.

Nonetheless, this method was restricted by the electric conductivity of the coating. Lee et al. fabricated superhydrophobic surfaces with micro Si column constructed above Au nano-cluster [16] or nano-pits on the Si micro-column sidewall [17], which can increase the gas fraction on the surface and extend the superhydrophobicity. These studies confirmed that nanostructures fabricated on or underneath a microstructure can effectively enhance the underwater hydrophobic stability. In our previous work, we prepared a surface with microsized polyvinylidene fluoride (PVDF) fibers on the TiO_2 nanorod arrays by hydrothermal and electrostatic spinning [18]. The prepared double gas layer surface can even withstand a water jet pressure of 250 kPa. However, the mechanical strength of the above surfaces, which were obtained by etching or in-situ growing on the inorganic surface, was not sufficient withstand friction or scratching. Despite many recent advances in this area, it is highly desirable to design stable multilayered micro/nanostructures by using high-strength polymers to enhance the durability of superhydrophobic coatings.

Epoxy (EP) resin are widely employed in industrial production due to their stable physicochemical properties, self-healing ability, and excellent adhesion to a metal substrate [19–21]. However, considering the hydrophilicity of EP resins, their hydrophobization with low surface energy materials is a crucial step to prepare superhydrophobic EP composite coatings. Owing to its lowest surface tension (19 mJ·m^{-2}), polytetrafluorethylene (PTFE) has been widely used to prepare non-wetting coatings or to reduce the surface energy of the coating [22,23]. Peng et al. [24] have successfully prepared a superhydrophobic EP coating by fluorinating epoxy molecules and physically adding PTFE particles. The prepared coating was even able to withstand immersion in aqua regia for 60 min. However, the EP/PTFE coating exhibited a marked decrease (150 μm) in thickness after only 100 abrasion cycles. This is mainly due to the fact that the non-polar PTFE only exerts a relatively weak dispersion force, which results in a weak interfacial
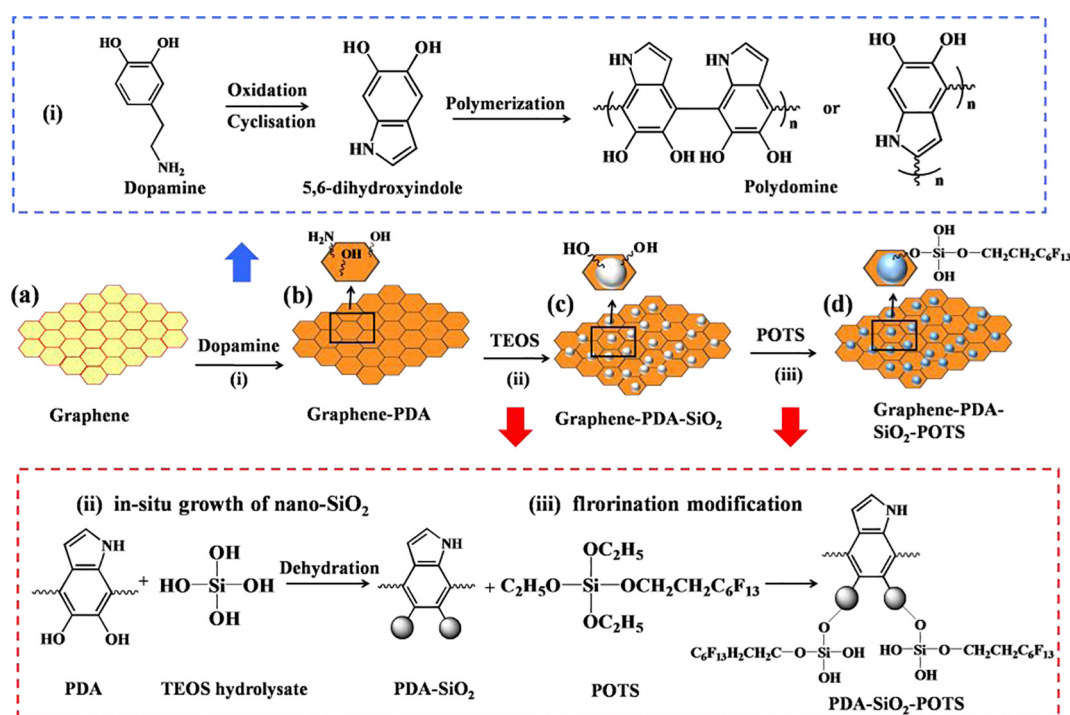

Fig. 1. The schematic diagram of the synthesis of GP-SiO$_2$-POTS particles.
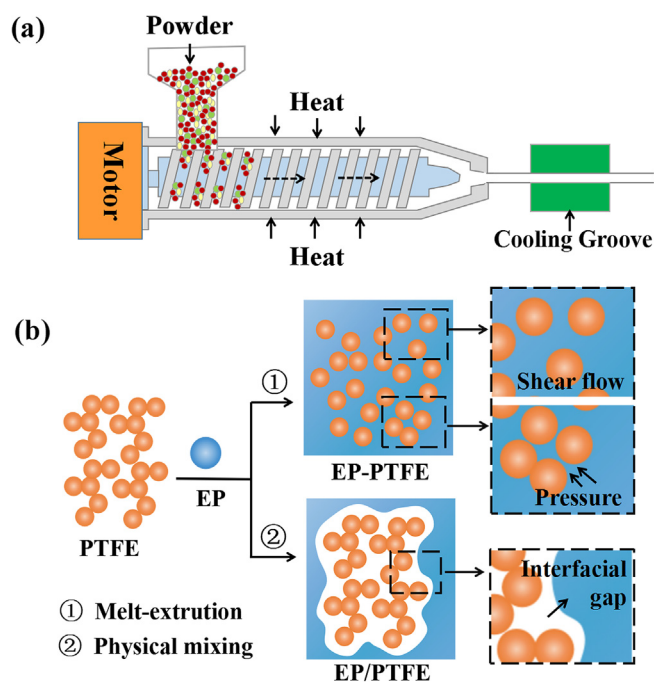
(a)

(b)

Fig. 2. The diagram of (a) melt extruder and (b) the process of melt-extrusion and physical mixing.

bond between PTFE and EP. Therefore, by enhancing the EP-PTFE interfacial bonding and designing a multilayered micro/nanostructure on the coating surface, it should be possible to prepare a superhydrophobic coating with durable hydrophobicity and mechanical properties.

To improve the EP-PTFE interfacial bond, we used melt extrusion to uniformly disperse PTFE particles in the EP, the bonding strength between PTFE and EP can be strongly enhanced by the twin screw extruder under high temperature, pressure, and shear force conditions. Moreover, mussel-inspired dopamine can provide a secondary functional platform on a solid surface via self-polymerization [25,26]. Thus, we used dopamine to provide a large number of active hydroxyl groups on the graphene surface. In combination with a sol-gel process, nano-silica particles can be grown in situ on the modified graphene to form graphene-polydopamine (PDA)-SiO$_2$ (GP-SiO$_2$) particles with three-dimensional (3D) structure. After modification with 1H,1H,2H,2H-per-fluorooctyltriethoxysilane (POTS), a superhydrophobic EP-PTFE/GP-SiO$_2$-POTS coating was successfully fabricated by electrostatic spraying without any solvent emission. Moreover, the lamellar structure of graphene can induce an even distribution of the nano-SiO$_2$ particles on both convex and flat coating surfaces. The prepared superhydrophobic coating with multilayered nano-micro-nano (NMN) structure demonstrated high hydrophobic stability and excellent wear resistance. This study is expected to introduce an effective way for preparing durable superhydrophobic coatings.

2. Experiment

2.1. Materials

Epoxy resin (EP) and curing agent were bought from Sinopec Group Baling Petrochemical Company. PTFE was obtained from Zhejiang Green New Materials Co., Ltd. (Zhejaing, China). Graphene (purity ≥ 99.5%, thickness ≤ 5 nm, and layer count ≤ 10) was bought from Nanjing Corfu Nano Corporation Beijing Marketing Center. Dopamine (purity ≥ 98%) and tris(hydroxymethyl) aminomethane hydrochloride (Tris-HCl) were supplied by Beijing Biotopped Science & Technology Co., Ltd. (China). Tetraethyl orthosilicate (TEOS) was obtained from Tianjin chemical reagent a factory·NH$_3$·H$_2$O (25%) was

purchased from Nanjing sambah biotechnology Co., Ltd, (China). 1H,1H,2H,2H-perfluorooctyltriethoxysilane (POTS) (purity ≥ 97.0%) was supplied by Weng Jiang chemical reagent Co., Ltd. (Guangdong, China). Ethyl alcohol was purchased from Tianjin yuanli chemical Co., Ltd. (China). Steel plate (Q235, thickness: 1 mm) was supplied by Tianjin LuBao steel sales Co. Ltd. Deionized water was obtained from Yongqingyuan pure water manufacturing center (Tianjin, China).

2.2. Preparation of GP-SiO$_2$ composite particles

Fig. 1 shows the preparation schematic diagram of function graphene particles. Firstly, 0.4 g graphene particles were added into 200 mL aqueous solution with 0.2 g dopamine (1 mg/mL) and 0.24 g Tirs. Graphene-polydopamine (GP) particles were obtained after stirring 24 h (500 r/min) and drying at 80 °C. Secondly, added 0.1 g GP particles into 15 mL of ethanol solution with 1 mL NH$_3$·H$_2$O and ultrasonic agitation 10 min. The mixture of 1 mL TEOS and 5 mL ethanol solution was added into GP solution dropwise and stirring 24 h (300 r/min) to complete hydrolysis. Finally, 50 μL POTS was added into the solution when the reaction goes to 18 h. GP-SiO$_2$-POTS particles were obtained after drying at 80 °C. The FT-IR and EDS spectra were used to confirm this reaction (Figs. S1–S3).

2.3. Preparation of EP-PTFE resin particles

Pure epoxy particles, curing agent and different content of PTFE were added into a premixer (150 rad/min). After 15 min, we added the obtained premixing EP/PTFE particles into twin screw extruder (SLG-30) with 200 rad/min (Fig. 2a). The screw has a diameter of 30 mm and a length of 450 mm. Through three-stage heating (85 °C, 95 °C and 105 °C), platy EP-PTFE can be obtained after cooling and crushing. Finally, EP-PTFE particles were prepared after the mill treatment.

2.4. Preparation superhydrophobic coating

10 g EP-PTFE particles with different mass of GP-SiO$_2$-POTS added into a small mechanical mixer and stir well. The mixture was sprayed on the steel plate (10 cm × 10 cm) surface by electrostatic spraying (80 kV voltage) with a spraying distance of 25 cm. EP-PTFE/GP-SiO$_2$-POTS coatings were obtained after calcing at 200 °C for 90 min.

2.5. Characterization

Surface morphologies of the prepared particles and coatings were observed by scanning electron microscope (SEM, Quanta 200). The morphologies of the prepared particles were measured by transmission electron microscope (TEM, JEM-2010). The chemical compositions were obtained by Nicolet 6700 infrared spectrometer. The elemental analysis was used by X-ray energy dispersive spectrometry (EDS) and X-ray photoelectronic spectroscopy (XPS-Thermo ESCALAB 250Xi). The water contact angles and sliding angles were measured by Contact Angle Meter (JGW-360A) with 5 μL water drops, respectively. The reported values were taken from the average of at least five measurements of the coating surface. The wear resistance was tested by a TABER abrasion tester. During the test, the prepared coating was fixed on the rotational platform and rubbed by the friction wheels, which were covered with 1000 mesh sandpapers and loaded with 500 g weight (*Technical Standard for Internal Fusion Bonded Epoxy Coating of Steel Pipe* SY/T 0442-2010). The thickness and adhesion strength were measured by a coating thickness gauge (SaluTron ComBi-D3, Germany) and cross-cut tester (QFH-2 mm), respectively.

3. Results and discussion

3.1. Analysis of GP-SiO₂ particles

The schematic diagram of the synthesis of GP-SiO$_2$-POTS particles is shown in Fig. 1. Under alkaline condition, dopamine can self-polymerize on the graphene surface and form a large amount of hydroxyl groups (Figs. S1 and S2). This can provide a secondary reaction platform for the growth of nano-SiO$_2$ particles during the sol-gel process (Fig. 1a–c). Compared with the smooth flake-like graphene surface (Fig. 3a), a large amount of nano-SiO$_2$ particles uniformly covered the graphene surface modified by 4 mM·L^{-1} PDA (Fig. 3b1, b2). However, the distribution of nano-SiO$_2$ particles on the modified graphene was discrete. Fig. 3c1 shows that dense nano-SiO$_2$ particles were successfully grown on the graphene surface modified with 8 mM·L^{-1} PDA. The difference in the quantity of nano-SiO$_2$ particles grown on the graphene surfaces is mainly due to that the high content of PDA, which can provide a higher number of reaction sites for the growth of nano-SiO$_2$. Moreover, various nanopore structures can be formed among the dense nano-SiO$_2$ particles, which favors the storage of higher amounts of low-surface-energy POTS. Therefore, the prepared graphene-8 mM·L^{-1} PDA-SiO$_2$ particles with 3D structure were used to establish a hierarchical structure on the coating surface and overcome the SiO$_2$ agglomeration caused by the physical mixing process (Fig. 3d).

Moreover, transmission electron microscopy (TEM) measurements were performed to inspect the morphology of the prepared particles (Fig. 4). As shown in Fig. 4a, the pure graphene particles exhibited a flake-like morphology. After the sol-gel process, dense nano-silica particles were tightly bonded with the PDA-modified graphene surface, despite having been subjected to a strong ultrasound treatment before the TEM measurements (Fig. 4b). In contrast, SiO$_2$ could hardly be detected on the unmodified graphene surface except for its edges (Fig. 4c). The differences in the distribution of SiO$_2$ are mainly due the fact that ultrasonic waves can easily break the weak van der Waals interactions between SiO$_2$ and graphene, whereas PDA can enhance the interfacial bonding strength between graphene and SiO$_2$ via the formation of chemical bonds. Therefore, the SiO$_2$ grown on the PDA-modified graphene surface can withstand the destruction by ultrasonic

waves.

3.2. Mechanical abrasion of EP-PTFE and EP/PTFE composite coatings

Owing to their lowest surface tension (19 mJ·m^{-2}), PTFE particles have been widely used to prepare non-wetting coatings by physical mixing [27]. However, the non-polar surface of PTFE, without orientation or inducing forces, can hardly be adhesive to other resins, such as EP and polyester ones. Melt extrusion, as a solvent-free process, can overcome the cohesive resistance of the agglomerated PTFE particles and the interfacial resistance between PTFE and EP by shear flow and differential pressure flow [28,29]. Herein, a Taber abrasion tester (Fig. 5a) was employed to evaluate the mechanical stability of EP-PTFE (melt extrusion) and EP/PTFE (physical mixing), by measuring the abrasion loss.

Fig. 5b shows the abrasion losses of the physically mixed EP/PTFE coating and the hot-melt extruded EP-PTFE coating after 2000 abrasion cycles. The abrasion losses of all prepared coatings showed an initial decrease, followed by an increase. The significant reduction of abrasion losses was mainly ascribed to the low friction coefficient of PTFE, which can form a lubrication film on the sandpaper surface. The lubrication film changes the wear mechanism from micro-cutting to adhesion (Fig. S4), which can reduce the damage to the coating surface during the friction test [30]. However, once the PTFE content exceeded 5 wt%, the abrasion loss increased, especially for the EP/PTFE coating. As shown in Table 1, when the PTFE content was increased to 7.5 wt%, the difference in abrasion loss between EP/PTFE and EP-PTFE increased to 19.9 mg. Moreover, as the PTFE content was increased to 10 wt%, the difference further increased to 21.8 mg. As the composition of the materials is the same, this difference mainly depends on the enhancement of the interfacial strength between EP and PTFE by melt extrusion. Furthermore, numerous grooves and pits were observed on the surface of the EP/PTFE (7.5 wt%) coating after 2000 abrasion cycles (Fig. 5c). In contrast, the rubbed EP-PTFE (7.5 wt%) surface was relatively compact and smooth (Fig. 5d). The difference in surface topography further confirmed that high shear forces and pressures can effectively enhance the EP-PTFE interfacial bonding. Finally, according to the relation proposed by Cassie and Baxter ($\cos\theta^* = \sum f_i \cdot \cos\theta_i$) [31], a high
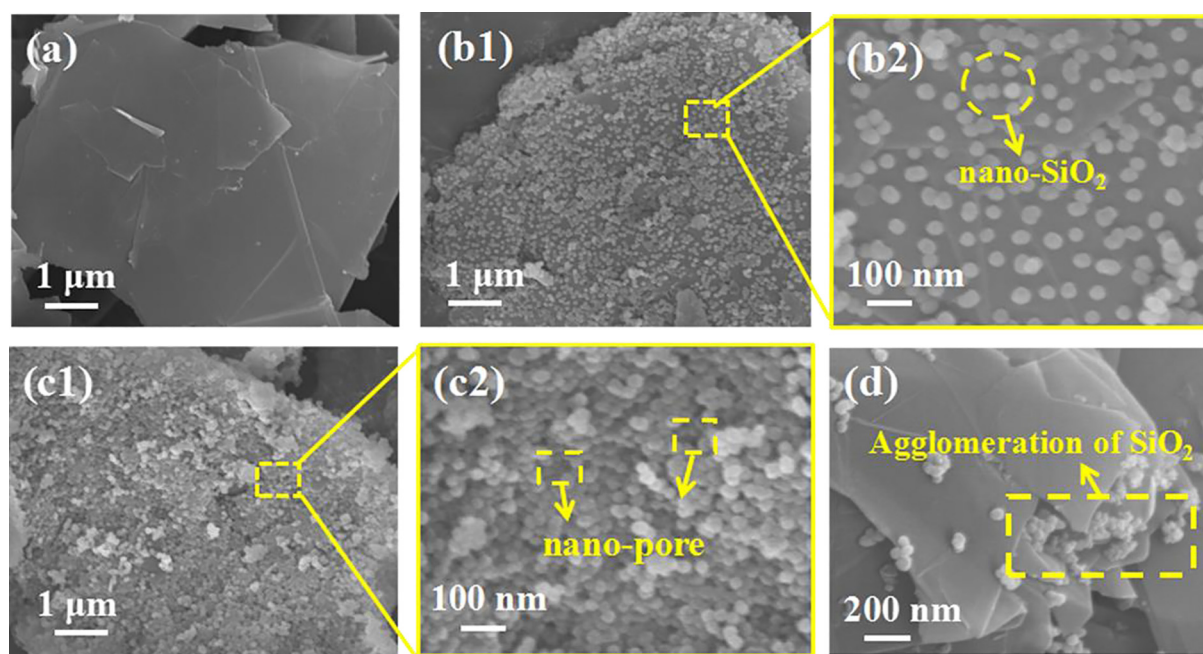

Fig. 3. SEM images of (a) graphene, SiO$_2$ in-situ growth on the (b1, b2) graphene-0.5 mg/mL PDA and (c1, c2) graphene-1 mg/mL PDA, (d) physical mixing of SiO$_2$ and graphene.
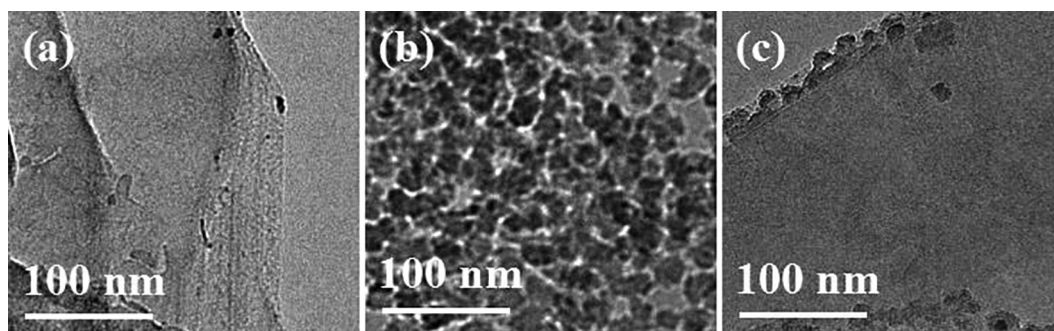
Fig. 4. TEM images of (a) graphene, (b) graphene-PDA-SiO$_2$, (c) graphene-SiO$_2$ without PDA.
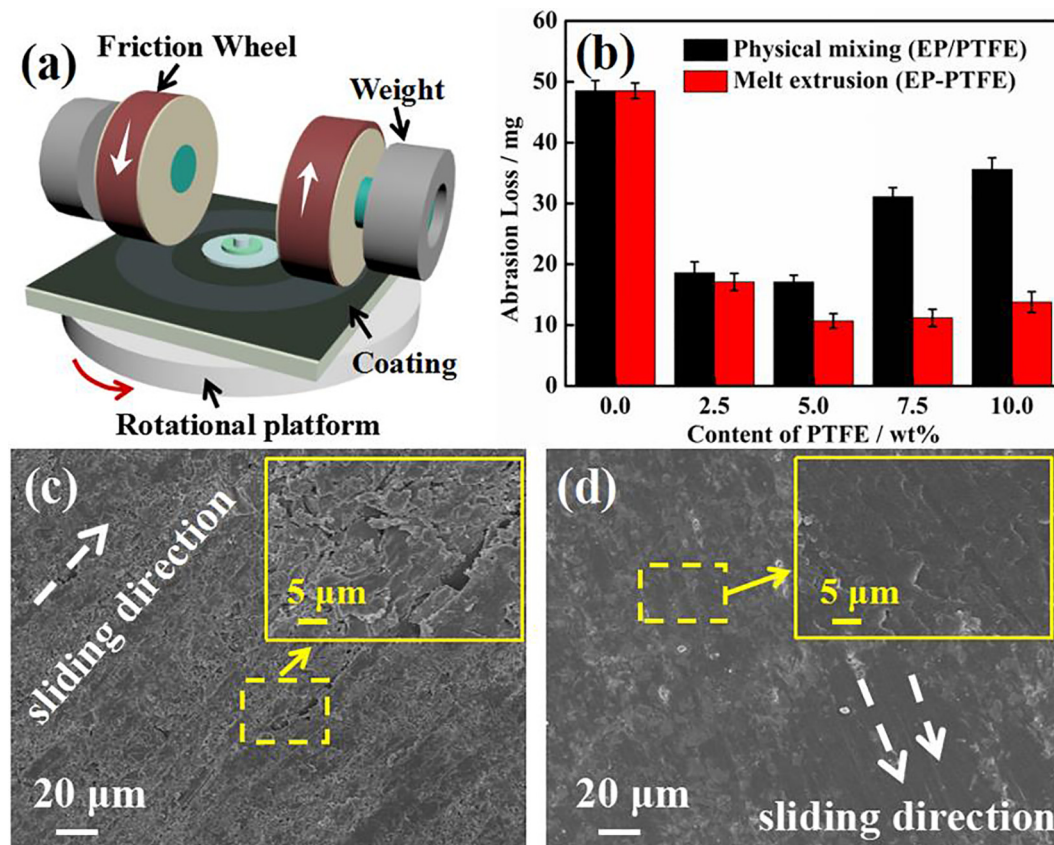

Fig. 5. (a) The schematic diagram of Taber abrasion tester, (b) The abrasion loss of EP/PTFE and EP-PTFE coating with different content of PTFE after 2000 cycles. The surface SEM images of (c) EP/7.5 wt% PTFE and (d) EP-7.5 wt% PTFE after 2000 abrasion cycles.

Table 1
The abrasion loss of EP/PTFE, EP-PTFE and the difference in abrasion loss after 2000 cycles test.

Content of PTFE	Abrasion loss/mg		
	EP/PTFE (physical mixing)	EP-PTFE (melt extrusion)	Δ mass
0	48.5	48.5	0
2.5 wt%	18.6	17.1	1.5
5.0 wt%	17.2	10.7	6.5
7.5 wt%	31.1	11.2	19.9
10 wt%	35.6	13.8	21.8

percentage of PTFE is more beneficial for improving the non-wetting properties of the coating. Considering the approximately equal abrasion loss of the EP-5 wt% and EP-7.5 wt% PTFE coatings, 7.5 wt% was chosen as the optimum added amounts of PTFE for preparing a durable

superhydrophobic coating by the melt extrusion process.

3.3. Wettability and surface morphology

Compared with the value of the pure EP surface, the WCA of the EP-PTFE surface increased from 84.3 ± 0.9° to 104.2 ± 1.2° (Fig. S5). To optimize the wettability, different contents of GP-SiO$_2$-POTS particles (from 0.2 to 1.4 wt%) were added to EP-PTFE. As shown in Fig. 6a, the prepared coating surface acquired superhydrophobic properties (WCA = 156.3 ± 1.5°, SA = 3.5 ± 0.5°) upon the addition of only 1 wt% of GP-SiO$_2$-POTS particles. Moreover, the WCA values showed no significant increase when the GP-SiO$_2$-POTS amount increased to 1.2 or 1.4 wt%. Considering that an excessive amounts of inorganic particles may impair the adhesion properties of the coating, EP-PTFE/1 wt% GP-SiO$_2$-POTS was chosen as the optimum superhydrophobic coating. The prepared coating also demonstrated high repellency against milk, juice, coffee, and tea (inset of Fig. 6a).
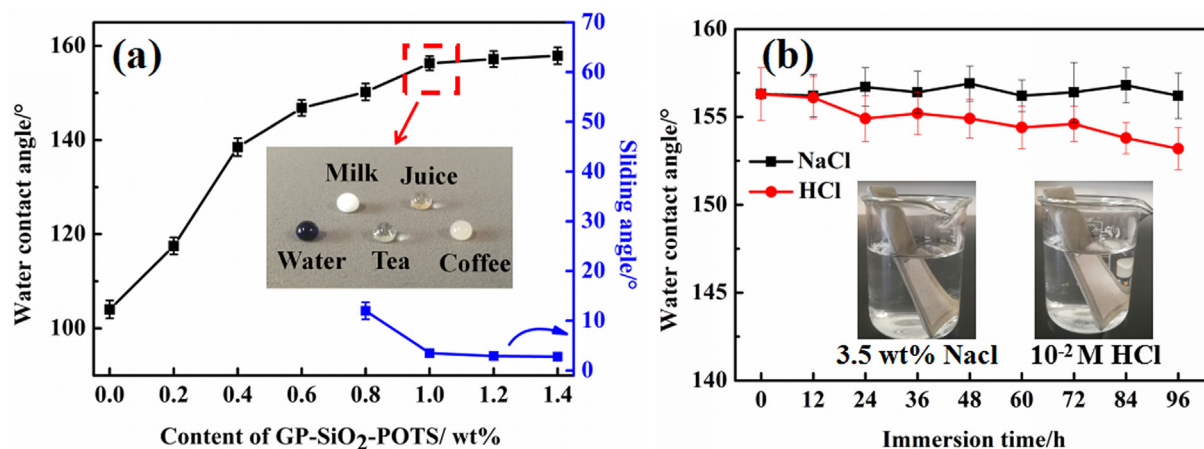
Fig. 6. (a) Effect of GP-SiO$_2$-POTS content on the wettability of EP-PTFE composite coating. (Inset: the wettability of milk, juice, water, tea, and coffee). (b) The change of WCA under different immersion time of 3.5 wt% NaCl and 10^{-2} M HCl. (Inset: the optical photos of immersion.).

Moreover, the EP-PTFE/GP-SiO$_2$-POTS coating was immersed into 10^{-2} M HCl and 3.5 wt% NaCl solutions to evaluate its hydrophobic stability, which is an important parameter to assess the performance of superhydrophobic coatings. Fig. 6b shows that the WCA of the prepared EP-PTFE/GP-SiO$_2$-POTS surface remained higher than 150° even after immersion in a 10^{-2} M HCl or 3.5 wt% NaCl solution for 96 h. The silver mirror effect of the coating surface was observed even after prolonging the immersion test time in the 3.5 wt% NaCl solution to 60 days. This time was much longer than that (less than 7 days) of other reported superhydrophobic coatings [32–35].

In order to analyze the difference in hydrophobic durability, the surface structures of the EP-PTFE/(1 wt%) GP-SiO$_2$-POTS and EP-PTFE/(1 wt%) graphene-SiO$_2$/POTS coatings are displayed in Fig. 7. The figure clearly shows a compact and uniform distribution of numerous nano-SiO$_2$ particles on the mastoid and flat portions of the EP-PTFE/GP-SiO$_2$-POTS coating surface (Fig. 7a1–a3). In contrast, the surface of the EP-PTFE/graphene-SiO$_2$/POTS coating consisted of smooth microscale structures and agglomerated nano-SiO$_2$ particles (Fig. 7b1–b3). The different surface structure of the two coatings can be ascribed to the different interfacial interaction between SiO$_2$ and graphene. Under the action of the polymer melt flow, the lamellar structure of graphene

promotes the uniform dispersion of the GP-SiO$_2$ particles on the coating surface. Therefore, the nano-SiO$_2$ particles grown on the graphene surface can be densely distributed on the surface of the coating and form a uniform nanostructure.

A schematic representation of the surface structure was plotted in Fig. 8. As shown in Fig. 8a1 and b1, the microsized mastoid portion forms the first protection barrier that prevents the entry of liquid. With increasing soaking time and water pressure, the water gradually squeezes into the pores of the microsized mastoids. Under such circumstances, the closely-arranged nanostructures can act as the second protection barrier to further prevent water penetration (Fig. 8a2), whereas the agglomerated nano-SiO$_2$ particles cannot achieve the secondary shielding effect (Fig. 8b2). Therefore, the EP-PTFE/GP-SiO$_2$-POTS surface with double air film protection possessed high hydrophobic durability in underwater conditions.

3.4. Self-cleaning and antifouling properties

In outdoor applications, the coating surfaces tend to accumulate gritty dirt or other contaminants. In this work, we selected sand as contaminants to test the self-cleaning properties of the prepared
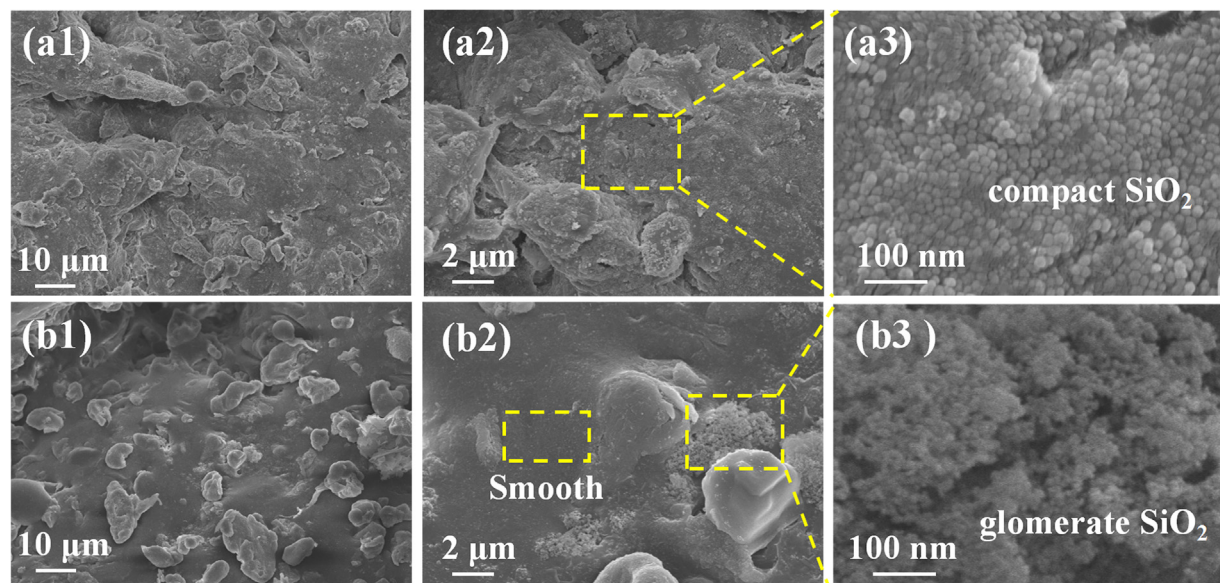

Fig. 7. SEM image of (a1, a2, a3) EP-PTFE/(1 wt%) GP-SiO$_2$-POTS coating surface and (b1, b2, b3) EP-PTFE/(1 wt%) graphene-SiO$_2$/POTS superhydrophobic coating without PDA.
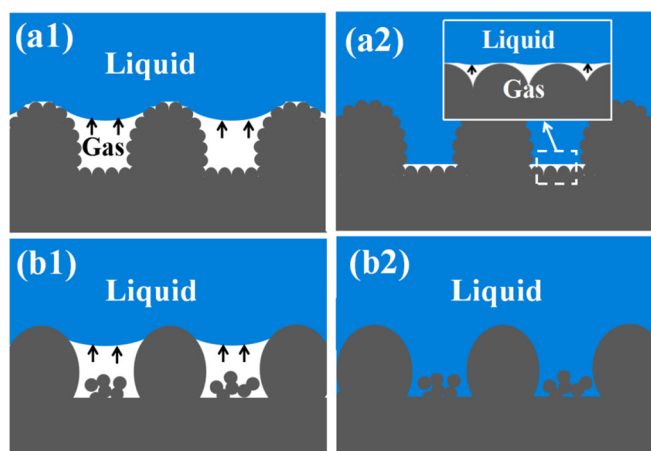
Fig. 8. Schematic representation of the surfaces structure with (a1, a2) and without (b1, b2) PDA modification.

superhydrophobic EP-PTFE/GP-SiO$_2$-POTS coating (Fig. 9a, b). As shown in Fig. 9b1, the EP-PTFE/GP-SiO$_2$-POTS coating covered with sand was tilted on the culture dish. Under the support of the surface hierarchical structure and the repulsion by the fluorinated groups, the water drops remains spherical and easily rolls off from the coating surface (Fig. 9a1). During this process, the sand is absorbed on the water drop surface and then removed from the coating surface (Fig. 9a2, b2), producing a clean coating surface after only a few rolling cycles (Fig. 9a3, b3).

The anti-fouling performance of the superhydrophobic coating is also an important parameter for outdoor applications. To mimic real pollution more closely, we prepared a slurry solution by mixing soil and water. Fig. 9c1 shows that when a steel plate was immersed into the slurry, the steel surface was in continuous direct contact with the slurry. After removing the plate, the glutinous slurry adhered to the surface and the steel plate was significantly polluted (Fig. 9b2). In contrast, the immersed EP-PTFE/GP-SiO$_2$-POTS coating trapped a stable air film between surface and slurry. This air layer can decrease the contact area and adhesion of the slurry on the coating surface (Fig. 9d1). Therefore, the prepared coating exhibited outstanding anti-fouling properties, and could repel the slurry solution to keep the surface clean even after 20 immersion times (Fig. 9d2).
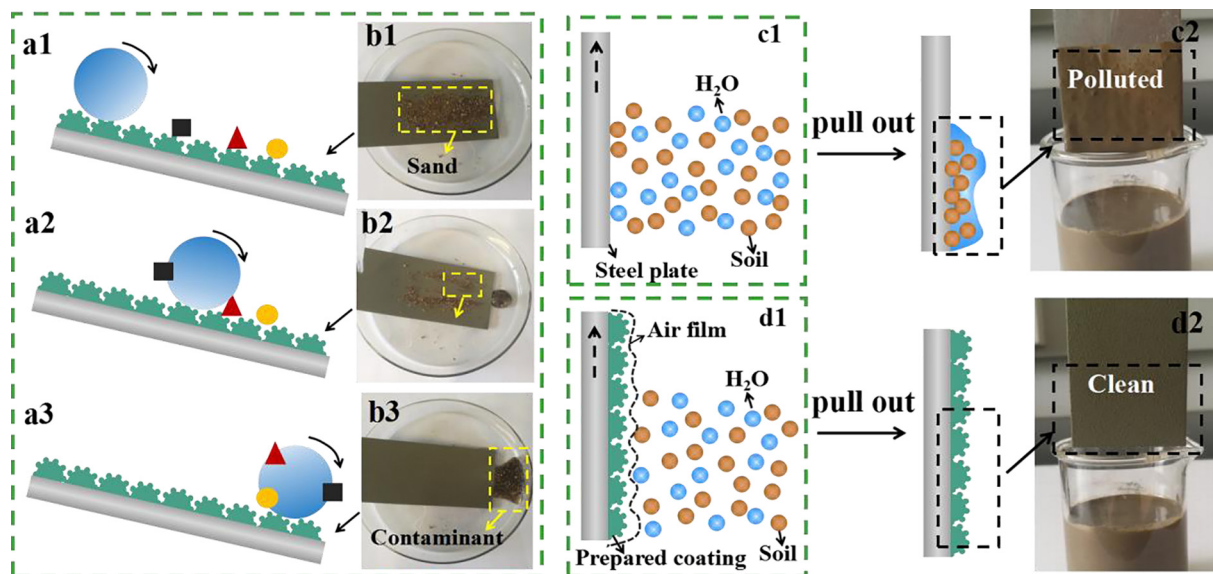
3.5. Mechanical robustness

As is well known, one of the biggest obstacles for the practical application of superhydrophobic coatings is the poor mechanical durability. Herein, a Taber abrasion tester with a 1000-mesh friction wheel and 500 g load was used to investigate the wear resistance of the coating, by measuring the abrasion loss and the variation in thickness. As shown in Fig. 10a, the initial thickness of the EP-PTFE/GP-SiO$_2$-POTS coating was 207 μm. After 100 abrasion cycles, the rubbed coating exhibited a slight decrease in thickness (18 μm), which was only about one-ninth of that (150 μm) reported for a physically mixed fluorinated EP/PTFE superhydrophobic coating [24]. It is worth mentioning that the load used in this test was twice that of the reported coatings. Moreover, after 2000 abrasion cycles, the decrease in thickness of the rubbed coating was still less than 50 μm. Therefore, the prepared EP-PTFE/GP-SiO$_2$-POTS coating possessed a stable mechanical strength.

In addition, Fig. 10a shows that the abrasion loss of the EP-PTFE/GP-SiO$_2$-POTS coating was only about 16.7 mg after 1000 rubbing cycles. Such a low abrasion loss can even satisfy the requirements of the technical standard for internal fusion bonded epoxy coatings of steel pipes in China ($\leq$20 mg, 1000 cycles). When the number of rubbing cycles increased to 2000, the abrasion loss only increased to 19.8 mg, which is much lower than those of the physically mixed EP/PTFE/GP/SiO$_2$/POTS coating (101.4 mg) and EP-PTFE/GP/SiO$_2$/POTS coating (25.2 mg) (Fig. S6). The significant improvement in the wear resistance of the EP-PTFE/GP-SiO$_2$-POTS coating can be mainly attributed to the dual interfacial enhancement provided by EP-PTFE and graphene-SiO$_2$ via the melt extrusion method and the PDA modification. Through this enhancement, the EP-PTFE/GP-SiO$_2$-POTS coating can withstand 10^5 abrasion cycles and shows a weight lose of only 54.4 mg after rubbing. The abrasion loss rate was also much lower than that of other reported non-superhydrophobic coatings [36–40] (Table S1).

Furthermore, we also investigated the influences of chemical and mechanical damage on the superhydrophobicity of the prepared coating. As shown in Fig. 10b, the WCA value remained above 150° after soaking in 0.1 M HCl for 30 min or finger touching. In addition, we also tested the alkali resistance of the prepared coating. The effect of the pH value on the wettability of the EP-PTFE/GP-SiO$_2$-POTS composite coating is shown in Fig. S7. After 30 min immersion in a strong alkaline solution (pH 14), the WCA of the composite coating showed a

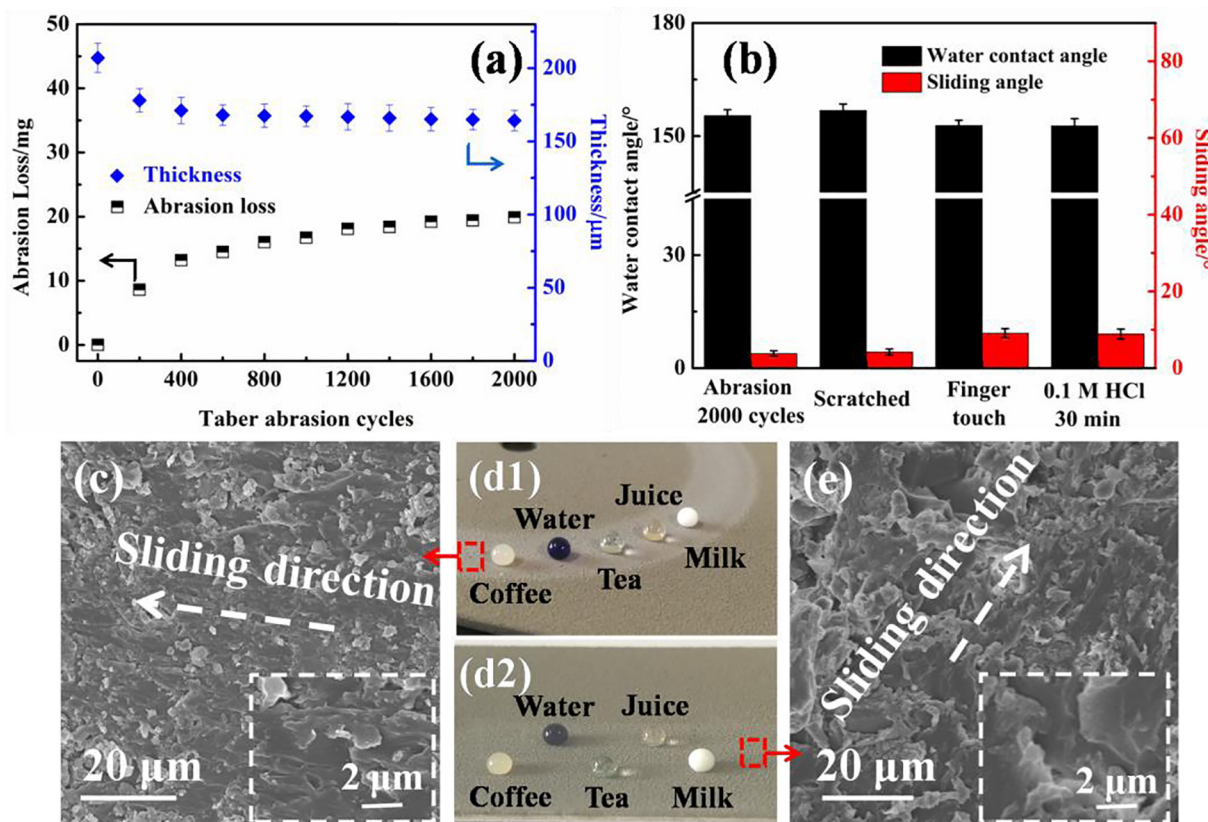
Fig. 9. Schematic (a1, a2, a3) and optical photograph (b1, b2, b3) of self-cleaning test with sand, antifouling tests of uncoated steel plate (c1, c2) and EP-PTFE/GP-SiO$_2$-POTS composite coating (d1, d2) by immersion into slurry.

Fig.10. (a) The change in abrasion loss and thickness with taber abrasion cycles, (b) The WCA after immersing in 0.1 M HCl 30 min, finger touch, scratched, abrasion 2000 cycles, The SEM images of (c) the abraded and (e) the scratched surface, the optical photograph of (d1) the abrasion and (d2) the scratched surface (inset, the wettability of milk, juice, water, tea, and coffee).
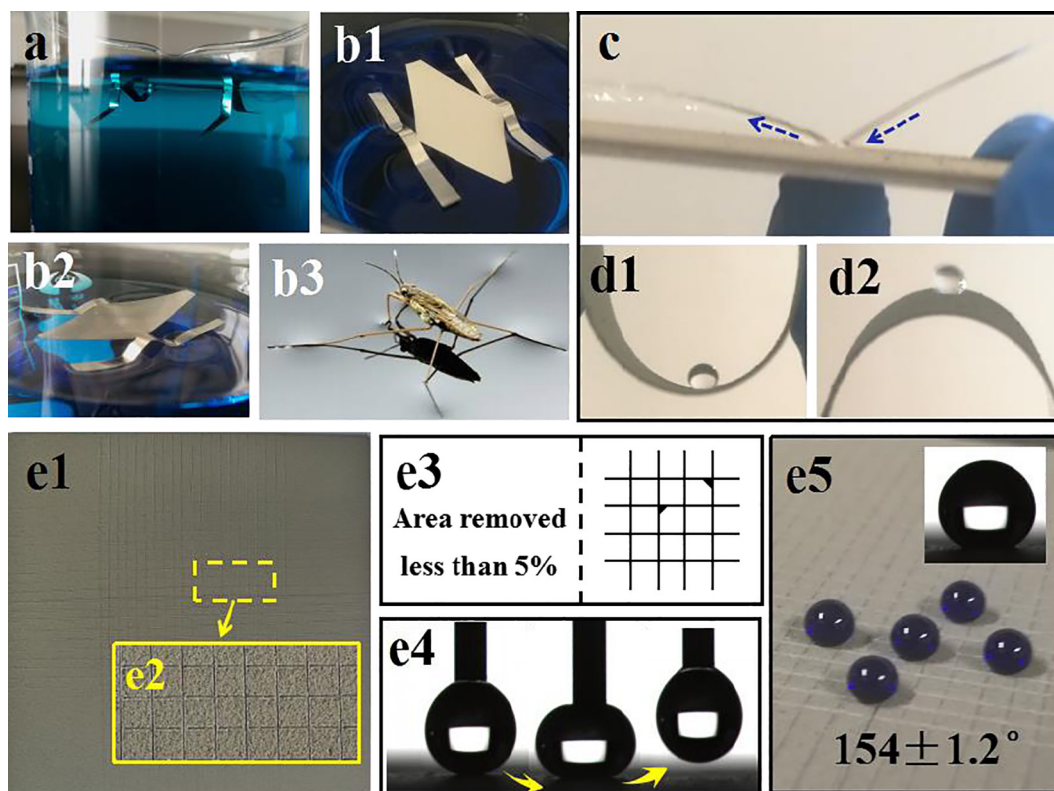

Fig. 11. (a) Uncoated strider-like steel dixsc on water, (b1, b2) A strider like steel disc with four "feet" on water covered with EP-PTFE/GP-SiO$_2$-POTS coating. (b3) Optical photo of strider. (c) Ejection, (d1, d2) Wettabiliy after bending and (e1, e2, e3, e4, e5) adhesion of EP-PTFE/GP-SiO$_2$-POTS coating.

marked decrease to 134 ± 2.3°. This is mainly due to the fact that the Si–O bond of POTS can be destroyed by a strong alkaline solution. Nonetheless, the coating maintained a stable superhydrophobicity in a weak alkaline solution (pH 10), and is therefore suitable for use in strongly acidic and weakly basic environments. Moreover, even after knife scratching or rubbing with sandpaper for 2000 cycles, the damaged surface could recover its superhydrophobicity by heating at 150 °C for 10 min. The healing surface also demonstrated high repellency to milk, juice, coffee, and tea (Fig. 10d1, d2). This phenomenon is mainly due to the fact that the abraded or scratched surface can maintain its hierarchical structures, providing the roughness necessary for the superhydrophobicity, even though it differs from the original morphology (Fig. 10c, d). Furthermore, the pre-stored POTS in the porous structures of GP-SiO$_2$ can migrate to the damaged surface to restore the superhydrophobicity during heat treatment. The XPS results (Fig. S8) show that the F atomic content in the rubbed coating surface increased from 52.94% to 81.93% (close to the initial content of 86.5%) after heat treatment. Therefore, the prepared superhydrophobic EP-PTFE/GP-SiO$_2$-POTS coating possesses excellent wear resistance and stable superhydrophobicity even after chemical or physical damage.

3.6. Adhesion ability of EP-PTFE/GP-SiO$_2$-POTS coating

A water strider-like steel disc "robot" with four "feet" was designed. As shown in Fig. 11a, the uncoated robot can hardly stand on the water surface, and its four feet were instantly immersed in water. However, the robot coated with EP-PTFE/GP-SiO$_2$-POTS can easily stand and slide on the water surface, just like the real spider (Fig. 11b). This is mainly due to the superhydrophobicity of the feet, which can generate a strong repulsive force on the water surface. Thus, the robot can stand on the water surface only through its four feet. When the coating was set in contact with water, a stable air layer was formed on its surface, which reduced the fluid resistance and effectively reflected the jet water stream (Fig. 11c). In addition, the air layer remained on the coating surface and kept its superhydrophobicity even after repeated upward or downward bending tests (Fig. 11d1, d2). In addition, no cracking or stripping occurred on the bent coating surface (Fig. S9), indicating that the prepared superhydrophobic EP-PTFE/GP-SiO$_2$-POTS coating possessed high bending resistance and hydrophobic stability.

The "Paints and Varnishes-Cross-Cut Test for Films" (GB/T9286) standard test was used to evaluate the adhesion ability of the EP-PTFE/GP-SiO$_2$-POTS coating. As shown in Fig. 11e1, 2 mm × 2 mm grids were drawn on the prepared coating by a cross-cut tester. Then, high-tack tape (VHB, 3 M) was pasted on the cross-cut surface and the tape was pulled out in the vertical direction. This process was repeated until no debris remained on the tape. After the test, almost no flaking was observed around the cross-incision in Fig. 11e2. The test result corresponded to grade 1 adhesion, because the stripped area was less than 5% (Fig. 11e3). Moreover, the tested coating surface retained its superhydrophobicity, with a high WCA of 154 ± 1.2° (Fig. 11e4, e5). These outstanding adhesion properties can be mainly attributed to the enhancement of the interfacial bonding between PTFE and EP by the melt extrusion at high pressure. At the same time, the in-situ growth of SiO$_2$ on the GP surface can also enhance bonding at the interparticle interface and avoid the aggregation of nano-SiO$_2$ particles, which favors the cross-linking of polymers. Therefore, the superhydrophobic EP-PTFE/GP-SiO$_2$-POTS coating exhibited excellent adhesion ability, which can further expand its range of applications.

4. Conclusion

In this study, a robust superhydrophobic EP-PTFE/GP-SiO$_2$-POTS coating (WCA = 156.3 ± 1.5°, WSA = 3.5 ± 0.5°) was successfully prepared by electrostatic spraying. The interfacial bonding strengths of EP-PTFE and GP-SiO$_2$ were enhanced by the differential pressure shear flow during melt extrusion and the "glue" action of polydopamine,

respectively. This double interfacial enhancement significantly improved the mechanical properties of the prepared coating. In addition, the special NMN structure can trap a more stable air layer, preventing diffusion of water in the coating interior. The formed NMN structure can also create a second protection barrier to prolong the hydrophobic performance and maintain the surface clean during the self-cleaning and anti-fouling tests. The prepared superhydrophobic EP-PTFE/GP-SiO$_2$-POTS coating shows a promising application potential, due to its excellent wear resistance, self-cleaning, anti-fouling, and adhesion properties.

5. Notes

The authors declare no competing financial interest.

Appendix A. Supplementary data

Supplementary data to this article can be found online at https://doi.org/10.1016/j.cej.2019.04.038.

References

[1] P. Khanjani, A.W. King, G.J. Partl, L.S. Johansson, M.A. Kostiainen, R.H. Ras, Superhydrophobic paper from nanostructured fluorinated cellulose esters, ACS Appl. Mater. Inter. 10 (2018) 11280–11288.
[2] M.W. England, T. Sato, C. Urata, L. Wang, A. Hozumi, Transparent gel composite films with multiple functionalities: long-lasting anti-fogging, underwater super-oleophobicity and anti-bacterial activity, J. Colloids Interface Sci. 505 (2017) 566–576.
[3] S. Bengaluru Subramanyam, V. Kondrashov, J.r. Rühe, K.K. Varanasi, Low ice adhesion on nano-textured superhydrophobic surfaces under supersaturated conditions, ACS Appl. Mater. Inter. 8 (2016) 12583–12587.
[4] Z. Yang, L. Wang, W. Sun, S. Li, T. Zhu, W. Liu, G. Liu, Superhydrophobic epoxy coating modified by fluorographene used for anti-corrosion and self-cleaning, Appl. Surf. Sci. 401 (2017) 146–155.
[5] J. Gu, P. Xiao, P. Chen, L. Zhang, H. Wang, L. Dai, L. Song, Y. Huang, J. Zhang, T. Chen, Functionalization of biodegradable PLA nonwoven fabric as super-oleophilic and superhydrophobic material for efficient oil absorption and oil/water separation, ACS Appl. Mater. Inter. 9 (2017) 5968–5973.
[6] G.B. Hwang, A. Patir, K. Page, Y. Lu, E. Allan, I.P. Parkin, Buoyancy increase and drag-reduction through a simple superhydrophobic coating, Nanoscale 9 (2017) 7588–7594.
[7] P. Wang, T. Zhao, R. Bian, G. Wang, H. Liu, Robust superhydrophobic carbon nanotube film with lotus leaf mimetic multiscale hierarchical structures, ACS nano 11 (2017) 12385–12391.
[8] Y. Liu, X. Yin, J. Zhang, Y. Wang, Z. Han, L. Ren, Biomimetic hydrophobic surface fabricated by chemical etching method from hierarchically structured magnesium alloy substrate, Appl. Surf. Sci. 280 (2013) 845–849.
[9] Y. Liu, S. Li, J. Zhang, Y. Wang, Z. Han, L. Ren, Fabrication of biomimetic superhydrophobic surface with controlled adhesion by electrodeposition, Chem. Eng. J. 248 (2014) 440–447.
[10] S. Wang, X. Yu, Y. Zhang, Large-scale fabrication of translucent, stretchable and durable superhydrophobic composite films, J. Mater. Chem. A 5 (2017) 23489–23496.
[11] H. Ye, L. Zhu, W. Li, H. Liu, H. Chen, Simple spray deposition of a water-based superhydrophobic coating with high stability for flexible applications, J. Mater. Chem. A 5 (2017) 9882–9890.
[12] J. Ju, X. Yao, X. Hou, Q. Liu, Y.S. Zhang, A. Khademhosseini, A highly stretchable and robust non-fluorinated superhydrophobic surface, J. Mater. Chem. A 5 (2017) 16273–16280.
[13] X. Jing, Z. Guo, Biomimetic super durable and stable surfaces with superhydrophobicity, J. Mater. Chem. A 6 (2018) 16731–16768.
[14] Z. Liu, H. Wang, X. Zhang, C. Lv, C. Wang, Y. Zhu, Robust and chemically stable superhydrophobic composite ceramic coating repellent even to hot water, Adv. Mater. Interfaces 4 (2017) 1601202.
[15] J. Cheek, A. Steele, I.S. Bayer, E. Loth, Underwater saturation resistance and electrolytic functionality for superhydrophobic nanocomposites, Colloids Polym. Sci. 291 (2013) 2013–2016.
[16] C. Lee, C.-J.C. Kim, Maximizing the giant liquid slip on superhydrophobic microstructures by nanostructuring their sidewalls, Langmuir 25 (2009) 12812–12818.
[17] C. Lee, C.-J. Kim, Underwater restoration and retention of gases on

superhydrophobic surfaces for drag reduction, Phys. Rev. Lett. 106 (2011) 014502(1) 014502(4).

[18] Z. Liu, H. Wang, X. Zhang, C. Wang, C. Lv, Y. Zhu, Durable and self-healing superhydrophobic surface with bistratal gas layers prepared by electrospinning and hydrothermal processes, Chem. Eng. J. 326 (2017) 578–586.

[19] Y. Huangfu, C. Liang, Y. Han, H. Qiu, P. Song, L. Wang, J. Kong, J. Gu, Fabrication and investigation on the Fe_3O_4/thermally annealed graphene aerogel/epoxy electromagnetic interference shielding nanocomposites, Compos. Sci. Technol. 169 (2019) 70–75.

[20] X. Yang, Y. Guo, X. Luo, N. Zheng, T. Ma, J. Tan, C. Li, Q. Zhang, J. Gu, Self-healing, recoverable epoxy elastomers and their composites with desirable thermal conductivities by incorporating with BN fillers via in-situ polymerization, Compos. Sci. Technol. 164 (2018) 59–64.

[21] J. Gu, X. Yang, C. Li, K. Kou, Synthesis of cyanate ester microcapsules via solvent evaporation technique and its application in epoxy resins as a healing agent, Ind. Eng. Chem. Res. 55 (2016) 10941–10946.

[22] L. Shi, J. Hu, X. Lin, L. Fang, F. Wu, J. Xie, F. Meng, A robust superhydrophobic PPS-PTFE/SiO_2 composite coating on AZ31 Mg alloy with excellent wear and corrosion resistance properties, J. Alloy Compd. 721 (2017) 157–163.

[23] R. Liao, C. Li, Y. Yuan, Y. Duan, A. Zhuang, Anti-icing performance of ZnO/SiO_2/PTFE sandwich-nanostructure superhydrophobic film on glass prepared via RF magnetron sputtering, Mater. Lett. 206 (2017) 109–112.

[24] C. Peng, Z. Chen, M.K. Tiwari, All-organic superhydrophobic coatings with mechanochemical robustness and liquid impalement resistance, Nat. Mater. 17 (2018) 355.

[25] L. Tang, J. Dang, M. He, J. Li, J. Kong, Y. Tang, J. Gu, Preparation and properties of cyanate-based wave-transparent laminated composites reinforced by dopamine/POSS functionalized Kevlar cloth, Compos. Sci. Technol. 169 (2019) 120–126.

[26] C. Liang, P. Song, H. Gu, C. Ma, Y. Guo, H. Zhang, X. Xu, Q. Zhang, J. Gu, Nanopolydopamine coupled fluorescent nanozinc oxide reinforced epoxy nanocomposites, Compos. Part A 102 (2017) 126–136.

[27] D.S. Vernez, P.-O. Droz, C. Lazor-Blanchet, S. Jaques, Characterizing emission and breathing-zone concentrations following exposure cases to fluororesin-based waterproofing spray mists, J. Occup. Environ. Hyg. 1 (2004) 582–592.

[28] A.L. Sarode, H. Sandhu, N. Shah, W. Malick, H. Zia, Hot melt extrusion (HME) for amorphous solid dispersions: predictive tools for processing and impact of drug–polymer interactions on supersaturation, Eur. J. Pharm. Sci. 48 (2013) 371–384.

[29] J.C. DiNunzio, C. Brough, J.R. Hughey, D.A. Miller, R.O. Williams III, J.W. McGinity, Fusion production of solid dispersions containing a heat-sensitive active ingredient by hot melt extrusion and Kinetisol® dispersing, Eur. J. Pharm. Biopharm. 74 (2010) 340–351.

[30] M. Buchely, J. Gutierrez, L. Leon, A. Toro, The effect of microstructure on abrasive wear of hardfacing alloys, Wear 259 (2005) 52–61.

[31] J. Yong, F. Chen, Q. Yang, J. Huo, X. Hou, Superoleophobic surfaces, Chem. Soc. Rev. 46 (2017) 4168–4217.

[32] S. Khorsand, K. Raeissi, F. Ashrafizadeh, Corrosion resistance and long-term durability of super-hydrophobic nickel film prepared by electrodeposition process, Appl. Surf. Sci. 305 (2014) 498–505.

[33] Z. Wei, D. Jiang, J. Chen, X. Guo, Combination of chemical etching and electrophoretic deposition for the fabrication of multi-scale superhydrophobic Al films, Mater. Lett. 196 (2017) 115–118.

[34] E. Yousefi, M.R. Ghadimi, S. Amirpoor, A. Dolati, Preparation of new super-hydrophobic and highly oleophobic polyurethane coating with enhanced mechanical durability, Appl. Surf. Sci. 454 (2018) 201–209.

[35] S. Wan, Y. Cong, D. Jiang, Z.-H. Dong, Weathering barrier enhancement of printed circuit board by fluorinated silica based superhydrophobic coating, Colloids Surf. A 538 (2018) 628–638.

[36] L. Bonin, V. Vitry, Mechanical and wear characterization of electroless nickel mono and bilayers and high boron-mid phosphorus electroless nickel duplex coatings, Surf. Coat. Technol. 307 (2016) 957–962.

[37] A. Vilardell, N. Cinca, I. Pacheco, C. Santiveri, S. Dosta, I. Cano, J. Guilemany, M. Sarret, C. Muller, Hierarchical structures of anodised cold gas sprayed titanium coatings, T. I. Met. Finish 96 (2018) 71–78.

[38] K. Song, D. Chen, R. Polak, M.F. Rubner, R.E. Cohen, K.A. Askar, Enhanced wear resistance of transparent epoxy composite coatings with vertically aligned halloysite nanotubes, ACS Appl. Mater. Interface 8 (2016) 35552–35564.

[39] H. Naderi-Samani, R.S. Razavi, M.R. Loghman-Estarki, M. Ramazani, The effects of organoclay on the morphology and mechanical properties of PAI/clay nanocomposites coatings prepared by the ultrasonication assisted process, Ultrason. Sonochem. 38 (2017) 306–316.

[40] V. Vitry, L. Bonin, Formation and characterization of multilayers borohydride and hypophosphite reduced electroless nickel deposits, Electrochim. Acta 243 (2017) 7–17.